Small Aircraft Infrared Radiation Measurements Supporting the Engine Airframe Aero-thermal Integration

Jozsef Rohacs[1*], Istvan Jankovics[1], Istvan Gal[1], Jerzy Bakunowicz[2], Giuseppe Mingione[3], Antonio Carozza[3]

Abstract

The large, EU Supported ESPOSA (Efficient Systems and propulsion for Small Aircraft) project has developed new small gas turbines for small aircraft. One of the important tasks was the engine - airframe aero-thermal radiation integration that included task of minimizing the infrared radiation of the small aircraft, too. This paper discusses the factors influencing on the aircraft infrared radiation, its possible simulation and measurements and introduces the results of small aircraft infrared radiation measurements. The temperature of aircraft hot parts heated by engines were determined for validation of methodology developed and applied to engine - aircraft thermal integration.

Keywords

aircraft, infrared radiation, radiation measurements, engine - airframe thermal integration

[1] Department of Aeronautics, Naval Architecture and Railway Vehicles,
Faculty of Transportation Engineering and Vehicle Engineering,
Budapest University of Technology and Economics,
H-1521 Budapest, P.O.B. 91, Hungary

[2] Aviation Training Centre,
Rzeszow University of Technology,
al. Powstancow Warszawy 12, 35-959 Rzeszow, Poland

[3] CIRA Centro Italiano Ricerche Aerospaziali,
Via Maiorise 81043 Capua (CE), Italy

* Corresponding author, e-mail: jrohacs@vrht.bme.hu

1 Introduction

The infrared is an invisible radiant energy. This electromagnetic radiation has longer wavelength (starting from nominal red visible line wavelength 700 nanometers up to 1 mm), than the visible light. The first defense equipment for measuring the infrared radiation were developed prior the World War I. During World War II, the infrared detection was used for tracking, too (Hudson, 1969). The first missiles seeking the IR, i.e. infrared (thermal) radiation had been developed for beginning of 1950s, while, because the success of radar systems, its wide application was started about 10 - 15 years later. Titterton (2006) found from statistics that, the heat-seeking missiles had been responsible for more than 80 % of all the combat losses over 40 years since 1960s. During the Gulf war, (1991) IR (infrared) missiles were responsible for 76% of the neutralized aircrafts, while during the Kosovo war, the NATO aircraft were not allowed to fly below 15 000 ft, because the missiles effectiveness (Santos et al., 2007). On the same time, since 1987, for 26 years 35 civilian aircraft had been attacked by shoulder-fired missiles that caused more than 500 deaths (Bolkcom et al., 2004). (It is true, this large number might be less, because some lost civilian aircraft were used for military purposes, some others or better to say most of them were attacked in conflict zones, where they may have been perceived as being used for military purposes (Sweetman, 2003)). In any case, in 2003, Department of Homeland Security initiated – probably the first – large civilian project for detailing the implementation of an anti-missile system on a single commercial aircraft (Bolkcom et al., 2004).

The aircraft infrared radiation has investigated by many researchers, developers for the last 50 - 60 years as it summarized by Mahulikar et al. (2007). The most of research were and are related to military applications. For first period, the experimental studies had been focused on the military aircraft infrared signature measurement and aircraft type recognition, too. Later, the practical measurement of the civilian large aircraft infrared radiation signatures (Coiro et al., 2012), the radiation modeling and countermeasure became to set of important tasks. Parallel, to these, the infrared radiation sensor technology (Rogalski, 2012) has been developed rapidly, too. The information about

errors and uncertainties in the IR measurements could be found in Minkina et al. (2009).

The research can be divided into two major groups: investigation of the aircraft infrared signature (including the theoretical and practical studies) and sensing the infrared radiation. Both have the same objective target recognition. Several papers list the codes using in investigation of the aircraft infrared radiation (Coiro et al., 2012; McGlynn, Auerbach, 1997; Mahulikar et al., 2007) from SIGGE of Swedish Defence Research that can be applied to compute the aircraft infrared signature, especially effects from nozzles and plumes; trough the US code SPIRITS, NATO's NIRATAM validated on large set of military aircraft; code SIRUS generated by large companies Lockheed Martin UK INSYS and BAE Systems until commercial codes SE-WORKBENCH, Radtherm-IR, SAFIR and SEISM. The Belgium Defence establishment has developed an open-source code OSMOSIS for compute the ships infrared signature that can be applied to the Arial vehicles, too.

Nowadays, the small and personal air transportation system developing rapidly (Holmes et al., 2004; Piwek and Wiśniowski, 2016; Rohacs, 2007a; 2007b). The ESPOSA (2016) project had developed special small gas turbines for small aircraft. During optimization of the engine components and airframe integration the thermal conditions and the infrared radiation had been taken into account (Buonomo et al., 2013; Carozza et al., 2013; Hendrick et al., 2015; Veress, Bicsak and Rohacs, 2016). The helicopters flying at low altitude also could be treated by IR missiles (see for example (Jingzhou et al., 2014)).

This paper shows and discusses the results of the infrared radiation measurements.

2 The sources of the aircraft infrared radiation

The infrared radiation of aircraft is composed from the different sources (Fig. 1) including the radiation from the aircraft hot parts, radiation from the heated parts, reflections of the sun-, sky- and earthshines.

The infrared radiation like all electromagnetic radiation interacts with matter in a variety of ways (White, 2012):

- reflects - a wave from a surface (angle of reflection equals the angle of incidence),
- refracts - when the direction of a wave bends when passing between two transparent media with different propagation speeds (Snell's law),
- scatters - that occurs (in blue sky) upon interaction with particles whose size approaches the length of the wave,
- diffracts - interaction occurring around the edges of an obstruction,
- interferes - interaction in both a constructive and destructive manner,
- absorbs - when radiation is converted into another form of energy (mostly to heat),

- emits - from matter by conversion from another form of energy,
- transmits - propagation of the infrared radiation through a transparent medium (or vacuum),
- polarizes - when an electric field is partially polarized by reflection from dielectric.
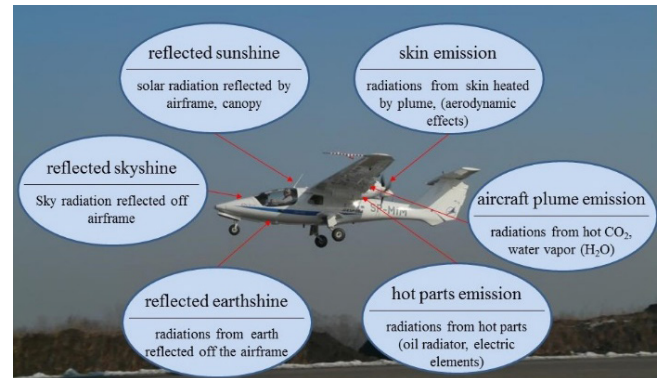

Fig. 1 Sources of aircraft infrared radiation (created by use of (Mahulikar et al., 2007)).

3 Governing laws

The aircraft infrared radiation that can be measured or sensed depends on heat sources, and intensity of sources (initiated by fuel burning (Bicsák, Hornyák and Veress)) aircraft real flight situation, inside and outside flow conditions and the infrared radiation itself. The last one is defined by the following - governing - rules (Siegel and Howell, 1972).

3.1 Planck's radiation law

It describes spectral radiance (L - energy per source *unit parameter*) that is emitted by a black body in thermal equilibrium at the defined (absolute) temperature (T). It can be given in different forms. For example the spectral radiance per unit of wavelength (λ) equals to

$$L(\lambda, T) = L_{e,\Omega,\lambda} \frac{2hc^2}{\lambda^5} \cdot \frac{1}{e^{hc/\lambda kT} - 1}, \qquad (1)$$

where k – Boltzmann constant: 1.38×10^{-23} J/K, h – Planck constant: 6.626×10^{-34} J·s, c – speed of light: 299 792 458 m/s. The SI dimension of the $L(\lambda, T)$ is W·sr^{-1}·m^{-3}. (Here sr is the SI unit of the steradian or square radian angle, Ω.).

3.2 Wien's displacement law

It defines the maximum wavelength (λ_{max}) at which the spectral radiance of black body radiation per unit wavelength is maximum, too.

$$\lambda_{max} = \frac{b}{T}, \ E_{max} = 1.309 \cdot 10^{-7} \cdot T^5, \qquad (2)$$

where b – Wien's displacement constant,
$$b = 2.8977721 \times 10^{-3} \, m \, K.$$

3.3 Stefan Boltzmann radiation law

Integration the Planck's distribution on the whole range of wavelengths ($\lambda = 0 \div \infty$) results to total energy emitted by a black body per unit surface area per unit time.

$$\dot{Q} = \int_0^\infty E(\lambda, T) \, d\lambda = \sigma \cdot T^4, \qquad (3)$$

where σ is the Stefan-Boltzmann constant,

$$\sigma = 5.67 \cdot 10^{-8} \, W / \left(m^2 K^4 \right).$$

3.4 Black body

A black body is defined as an ideal body that allows all the incident radiation to pass into it and absorbs internally all the incident radiation. This means no reflected and transmitted energy exist. This is true of radiation all wavelengths and for all angles of incidence. Hence the blackbody is a perfect absorber in incident radiation (Siegel and Howell, 1972).

Blackbody is an ideal of comparison for a body emitting radiation. A blackbody has two main properties in thermal equilibrium. First, it is an ideal emitter at every wavelength, it emits as much or more energy than any other body at the same temperature. Second, it is a diffuse emitter, which means that the energy is radiated isotopically, independent of direction.

The real body radiation can be given by its emittance or emissivity that is a ratio of real and black body radiations:

$$\varepsilon = \frac{E_{real}}{E_{black}}. \qquad (4)$$

The emissivity varies according to the surface properties, the material and, for some materials, also according to the temperature of the object. It also depends on the wavelength and angle of incidence.

For rough surfaces the value is close to unity, for polished surfaces it is around 0.02.

3.5 Kirchhoff's law of thermal radiation

The electromagnetic infrared radiation as usually hits the objects, while the objects absorb some of this energy. The value of absorptivity (α) is between 0 and 1, where 1 means a black body, 0 means a perfect white body.

The heated body, having higher temperature emits more infrared radiation than colder objects.

It is easy to understand that, in case of thermal equilibrium, when the temperature of a body is constant, i.e. independent on time, the emitted and absorbed radiation must be equal. Practically this means the body gives off as much energy as much absorbed:

$$\varepsilon = \alpha. \qquad (5)$$

3.6 Conservation of radiation energy

When the incident radiation reaches the surface of a material, it can act 3 ways depending on the material properties: it can be absorbed, transmitted and reflected. The absorbance (α) describes how much fraction of incidence radiation is absorbed, the transmittance (τ) is a measure of the ability of a material to transmit (allow through) infrared radiation. The reflectance (σ) is a measure of the ability of a material to reflect infrared radiation.

By use of energy conservation law the sum of absorbed, transmitted and reflected energy must be equal to the incident:

$$\dot{Q} = \alpha \cdot \dot{Q} + \tau \cdot \dot{Q} + \sigma \cdot \dot{Q},$$

or

$$\alpha + \tau + \sigma = 1. \qquad (6)$$

As transmission rarely plays a role in practice, the transmission (τ) is omitted and the formula is simplified to

$$\alpha + \sigma = 1$$

or because of Kirchhoff's law

$$\varepsilon + \sigma = 1.$$

This last equation allows determining the emissivity of the materials from its reflection that is easier to measure.

This short summary of governing rules contains all the required "radiation" equations applying in aircraft infrared radiation simulation, measurements and countermeasures. The other models are given by special studies and papers. For example, the basic equations of the fluid mechanics are summarized in (Buonomo et al., 2013; Veress, Bicsak and Rohacs, 2016). One of the recent examples of in-flight testing concerning measurement of boundary layer by infrared means might be found in Boden et al. (2015).

4 Practical aspects

According to the knowledge on (i) material properties, (ii) user manuals and guides of infrared videos (see for example (Pocket, 2012)) and (iii) our practice with developing the thermographic evaluation methods the following important practical aspects must be underlined.

There are some aspects according to the emittance: (i) for real bodies $\varepsilon < 1$, because real bodies also reflect and possibly transmit radiation; (ii) many non-metallic materials (e.g. PVC, concrete, organic substances) have high emissivity in the longwave infrared range that is not dependent on the temperature ($\varepsilon \approx 0.8 - 0.95$); (iii) metals, particularly those with a shiny surface, have low emissivity that fluctuates with the temperature; (iv) ε must be set properly for accurate measurement.

Another important comments on reflectance are (i) σ depends on the surface properties, the temperature and the type of material; (ii) in general, smooth, polished surfaces reflect more strongly than rough, matt surfaces made of the same material; (iii) the temperature of the reflected radiation must be taken into account (Reflective Temperature Compensation - RTC) that in many measurement applications corresponds to the ambient temperature (mainly in indoor thermography); (iv)

the RTC can be determined using a Lambert radiator (when the incident radiation is reflected with equal strength in all directions like the black bodies) and (v) the angle of reflection of the reflected infrared radiation is always the same as the angle of incidence, (similar to the reflection in optic).

Other comments according to the transmittance are (i) dependence on the type and thickness of the materials and (ii) the fact, the most materials are not transmissive, i.e. permeable, to long-wave infrared radiation.

Generally, there are two types of reflection can be distinguished, the specular and the diffuse reflections.

Specular reflection is a mirror-like reflection of electromagnetic waves (Fig. 2). In the optics the specular reflection means that light reflects off surfaces in a very predictable manner in accordance with the law of reflection: angles between the surface normal and incident and normal and reflected radiation are the same. In thermography it means that the heat source in the background is clearly visible on the surface because of specular reflection. The other result of this kind of behavior that the reflected picture of radiation sources highly depends on the angle of view. By changing the angle of view the reflected background can be optimized.
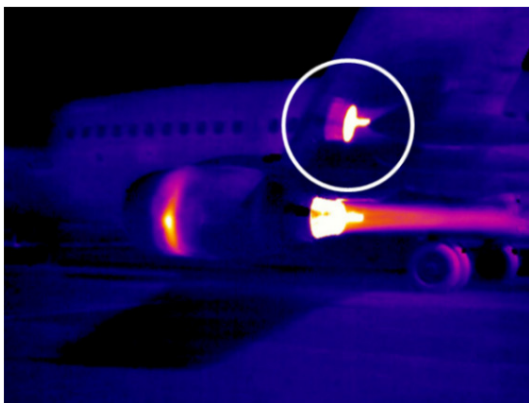

Fig. 2 CFM56 engine exhaust reflection on the wing bottom surface

Diffuse reflection is a reflection of rough surfaces. The roughness of the surface means that each individual ray of incident radiation reaches a surface which has different orientation. The normal lines at each point of incidence of rays are different for different rays. So the reflected radiation is scattering depending on the surface roughness. It means, with given accuracy of measurement of incident radiation, the error of measurement of emitted energy will be proportionately higher for reflective surfaces. Accurate measurement requires precise determination of emissivity values.

Finally, the Lambert's cosine law says that the radiant intensity observed from an ideal diffusely reflecting surface is directly proportional to the cosine of the angle between the surface normal and the direction of observer.

The emissivity may vary from 0.02 (aluminum, not oxidized at 25 °C) up to 0.94 (glass - 90 °C).

The accuracy of the thermo radiation measurements depends on the environmental conditions, too. The clouds, precipitation, air humidity, air flows, air pollution, etc.

The objectives of the thermo radiation measurements are the evaluation of influence of aircraft structural solutions and their possible optimization for reducing the infrared radiation.

Our practice going back to the end of the last century (Oravecz et al., 2000), and it showed that even relatively simple infrared cameras (like AGA Thermovision 750 type working with a special video recorder used in first investigations) can be applied to measurement, analysis and evaluation of the aircraft infrared radiations. As example, the Fig. 3 demonstrates the changes in infrared signature of an military helicopter after equipping with a special thermal emittance reducer. The photos were made in 1998, at the same flight conditions, from same distance, about the same military helicopter without (upper photo) and with (lower picture) equipment for IR reduction. The photos demonstrate that, the infrared radiations origins from all the heated parts of helicopters. The left photo shows the radiation reflected from the rotor blades that origins from the helicopter itself.
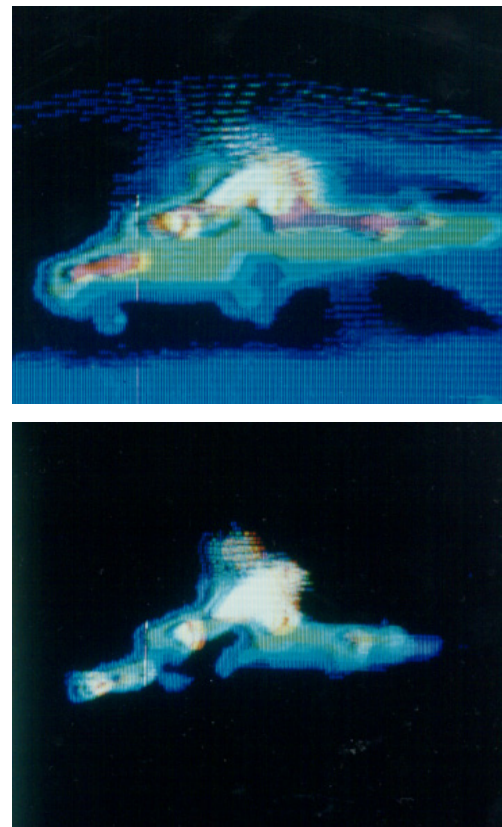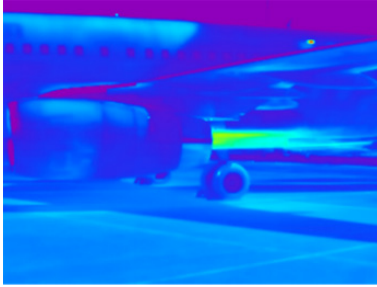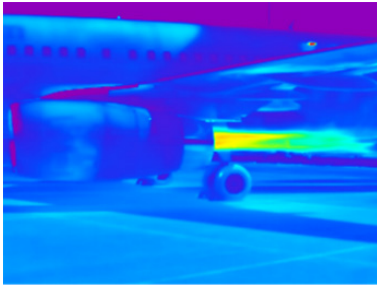

Fig. 3 Infrared radiation of a military helicopter without (upper) and with the thermal emittance reducer (lower image)

During preparation for measuring the infrared radiation of ESPOSA (2016) small demonstration aircraft, there were realized several measurements with use of a small gas turbine research stand and there were analyzed the changes in nacelle surface temperature and engine airframe integration of a middle size commercial aircraft.
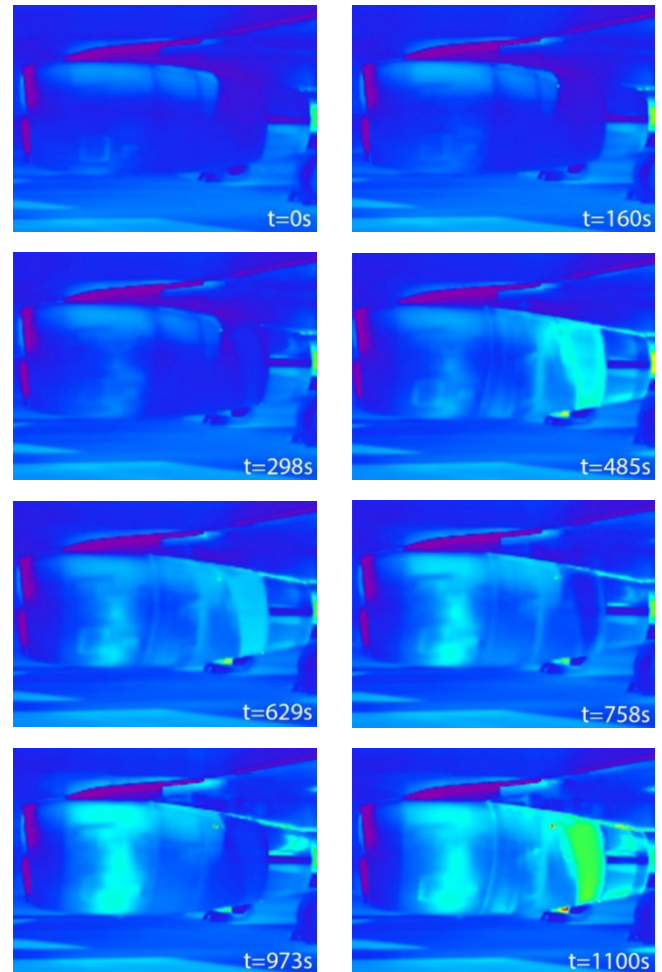
The Table 1 contains explanation and pictures of infrared radiation of engine nacelles and plumes.

The Fig. 4 and 5 show the changes in temperature of nacelle surface during the engine tests. As it can be seen, the temperatures measured at the M2 and M3 points are correlated by the N1 engine rotation speed (that - in Fig. 4 - given as % of maximum - take off – speed).
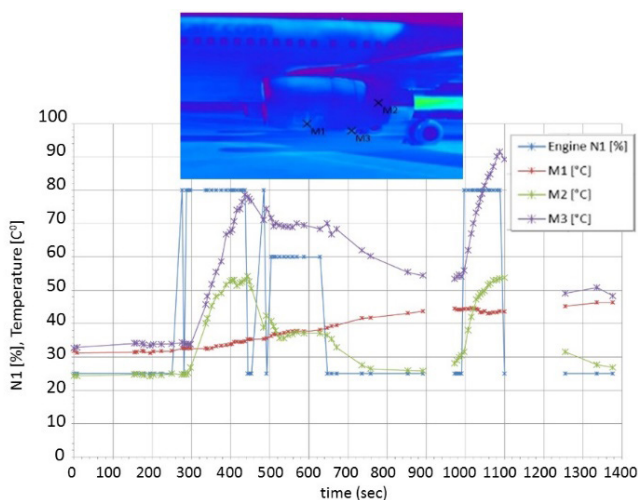
Table 1 Engine nacelle and plum radiation

Engine at low RPM (engine rotation speed - revolution per minute), the exhaust plume on thermal picture is short, with moderate temperature.	
Engine during RPM increase, the edge of exhaust is smooth while its length has increased, and relatively high temperatures can be observed in the core.	
Engine at high RPM, length of exhaust is long, edges are sharp, temperatures in the core are higher, but not as high as during the transition.	

Fig. 4 Points in which the nacelle surface temperatures are measured (in time interval with no measured data, the camera was moved to make measurements from different point of view)

The Fig. 5 shows eight thermo images of the nacelle that were selected with nearly same time intervals, to show how changing the temperature of engine nacelle during the 1100 seconds long time period.

Fig. 5 Infrared pictures of an engine nacelle at engine test (time is sec after starting the test)

5 Radiation simulation

The radiation simulation is a rather complex task, because it depends on the internal/external heat sources (as gas turbine, exhaust gas, oil radiators, hydraulic actuators, electric equipment, sunshine, etc.), internal/external flows (engine-airframe integration), infrared radiation, ray reflections and so on. In open and available references all these aspects are investigated.

One of the first simulation model of the aircraft infrared signature, the NIRATAM (the NATO Infrared Air Target Model) was developed by the NATO AC 243, Panel IV, Research Study Group 6 (RSG-6), for beginning of 1990s' (Noah et al., 1991). It was based on theoretical studies, field measurements, and infrared data analysis performed over many years. The vehicle fuselage, facet, model includes radiation due to aerodynamic heating, internal heat sources, reflected sky, earth, and solar radiation. Plume combustion gas emissions were calculated for H_2O, CO_2, CO, and other gases as well as solid particles. The developed software

generated graphical outputs of the target wireframe, plume flow field, atmospheric transmission, total signature and plume signature. This methodology is well applicable today, too.

The early 1990 several general models were developed. For example, the SPIRITS as spectral and in-band radiometric imaging of targets and scenes in a modeling software could be applied to model targets of a generic aircraft (Miller, 1993).

Already in 1998, Joyner et al. (1998) and his colleague created a generalized model, namely they integrated three IR models: Spectral In-Band Radiance of Targets and Scenes (SPIRITS), Physically Reasonable IR Signature Model (PRISM), and IR Electro-optical Naval Engagement (IRENE) into sensor simulator.

For the beginning of the new century, the complex modeling using the CFD results as inputs had been developed (Andersson, 2002).

a) The calculation of the aircraft infrared radiation and signature simulation depends on the objectives. The most used objective is the simulation of the IR signature from the recognition point of view (Santos et al., 2007; Willers and Willers, 2012). According to this, there are several important key considerations and aspects determining the creation of the required models and the simulation methodologies should be taken into account.

The key considerations identified by Willers and Willers (2012) for such an imaging infrared simulation system are: (i) radiometric accuracy in all spectral bands, (ii) accurate emitting source surface temperature behavior, (independently on the heat sources), (iii) high fidelity geometrical and spatial texture modeling, (iv) true dynamics and kinematic behavior (in six degrees of freedom), (v) detailed modeling of signatures and backgrounds, (vi)) accurate atmospheric transmittance and path radiance models, (vii) realistic rendering of the scene image in radiometric, spatial and temporal terms, and (viii) comprehensive sensor modeling to account for primary and second order imaging effects.

These key factors determine the requirements to develop the simulation models. The following aspects define the required modeling approaches from the (i) image recording, (ii) environmental conditions (as humidity) (iii), aircraft flight condition (spatial orientation), (iv) radiance and (v) reflection simulation point of view.

b) Sensor work. The sensors collect images for each wave number, η ($\eta = 1/\lambda$), therefore the radiation must be determined for all spectral band.

c) Sensing feature. The sensors record series of rays separated from the neighboring rays with angles of $\Delta\theta$ and $\Delta\phi$ (see Fig. 6.a).

d) Distance effect. Generally, the receivers sense the radiant flux (Φ_e radiant energy emitted, reflected transmitted or received per unit time) in form of radiant intensity (I – flux per steradian angle) and/or irradiance (i.e.

area power density at the receiver, E – flux per unit area). Irradiance and intensity are related by the square of the distance: $E = I/R^2$.

e) Projected area of source. According to the previously described definitions and aspects, the sensor elements "look at" the areas as spherical areas defined by the steradian angles, Ω (Fig. 6.b). That means the projected areas might be defined to all the aircraft surface elements as the solid body facet model elements that will be perpendicular to lines connecting them to the sensor elements. The angle between the normal to sensor plane and connecting line, θ_{real} and spatial position of the surface elements define the projection areas, A_{proj}.

f) Aircraft position. The measurable radiance depends on real position of aircraft. At first the heated elements of the aircraft can be "seen" by receivers directly, or partly, or even the heated elements can be in "shadow"of other aircraft elements. On the other hand, it is easy to understand the reflection of the sunshine, skyshine and earthshine really depends on the position of aircraft related to the sensor position.

g) Atmospheric filtration effects. The molecules and particles present in the atmosphere filter out some part of thermal radiation. For example, the infrared radiation generated by the fighter tailpipe and the plume is mostly contained in range of wavelength 3 to 5μm. The measurement (Santos et al., 2007) shows that, the radiant spectral emittance in the given range of wavelength is nearly zero with two large peaks (about 40 – 70 times greater values) in range between 4.17 - 4.20 μm and 4.32 - 4.70 μm.

h) Absorptivity. The atmospheric filtration effect can be determined by use of absorptivity of gases. The spectral transmissivity and absorptivity in a homogenous isothermal gas cell can be given by use of absorption coefficient, K_η,

$$\tau_\eta = e^{-K_\eta s}, \quad \alpha_\eta = 1 - e^{-K_\eta s},$$

where s is a thickness of the gas cell. Because the absorption coefficient depends on the contents of the gas cells, therefore the absorption coefficient is the sum of coefficients defining the gas cells with given concentration of the elements as CO_2, H_2O, etc. (Andersson, 2002). The coefficients might be determined from the (Rothman, 2013).

i) Modeling aspects. Actually, the aircraft infrared signature measuring is based on the radiant intensity or irradiance measurements (see sub point c)) that are analogous to radar cross section (RCS) detection or simulation (see for example (Rohacs, Palme and Sket, 2010; Palme et al., 2010; Perotoni and Andrade, 2011)). However there is a principal difference in analogies between IR and radio frequency (RF) because the target aircraft in the IR is an active emitter rather than the passive reflector of a distant RF illuminator. For this reason, intensity is actually more closely related to
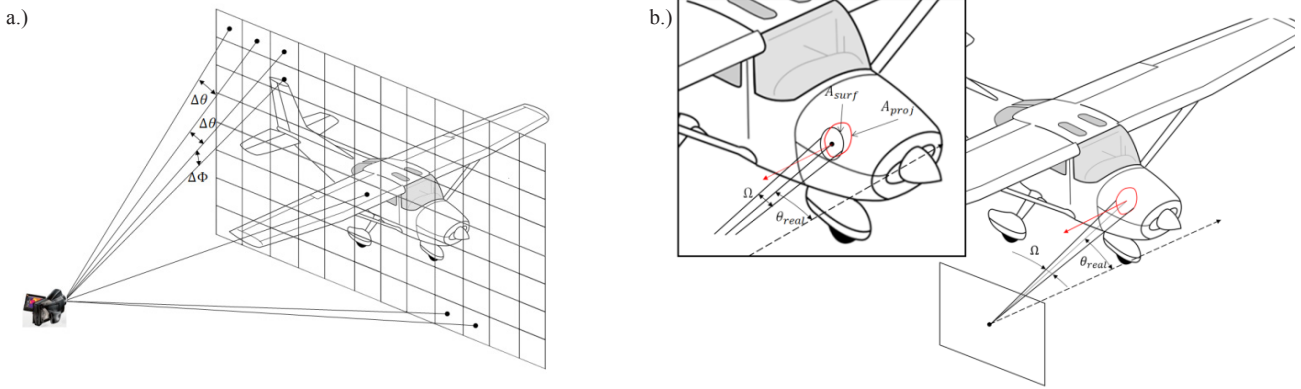
Fig. 6 Thermal radiation rays drawn from sensor point of view (a. (left side) - sensing the neighboring rays by steps of $\Delta\theta$ and $\Delta\phi$, b. (right side) - the sterian angle, Ω and measured surface, A_{surf} and projection area, A_{proj})

RF effective radiated power (ERP), which combines transmitter power with antenna beam (White, 2012).

j) Complexity. There are several methodological approaches to determining the infrared signature of aircraft. The complexity of the problem, simulation the infrared signature, can be characterized by one of the first code developed by Aerodyne Research Inc. (USA) in 1989 already to simulate long-range air-to-air detection and tracking engagements. The code integrated eight standalone modules (Iannarilli, Wohlers, 1991): (i) SPIRITS (aircraft IR signatures imaging module), (ii) CLOUD (sky background imaging module), (iii) LOWTRAN, (iv) TRACKER (signal processing and tracking module), (v) IPAS (optical sensor and spatial processing module), (vi) MISSION (dynamic trajectory module), (vii) ENGAGER (integrates all modules), and (viii) HIGH-LEVEL SCENARIO SPECIFIER (user-interface module).

k) Simulation aspects, inputs. The inputs often classified as (Davis and Thomson, 2002) (i) background information (geography, date and time, meteorological inputs), (ii) platform characteristics (size, shape, materials, coating, propulsion and auxiliary equipment) and (iii) threats (wavelength band, spatial resolution as scanner, imaging, etc., and sensitivity including detector noise). Here the platform might be the critical elements, because the applied materials and especial their coating and painting (Mahulikar et al., 2006) and fuselage skin heated by engine thermal processes. The last one can be determined by use of model developed by Mahulikar and his colleague (Mahulikar et al., 2001; 2005) that incorporates the radiation interchange in engine layout, to compute the temperature distribution of rear-fuselage skin for given engine operating conditions. The third platform problem is associated by engine exhaust plume that is well analyzed by (Mahulikar et al., 2007). Of course, the exhaust plume radiation together with the real fuselage play deterministic role in case of military aircraft and sensing from the real side. During operating the after burner system, the plume might be longer then the fuselage.

l) Methodology. Most of the simulation methods combine the computation fluid mechanics thermal condition calculation radiation emission and radiation reflection (Mahikular et al., 2001; Anderssen, 2002; Jianwei and Qiang, 2009; Pan et al., 2011).

The ESPOSA (2016) project studied the infrared radiation of small aircraft by use of two major methodologies. The theoretical investigations had objectives aero-thermal analysis and evaluation of the engine airframe integration and reducing the temperature distribution (by this infrared radiation) of the airframe elements heated by working engines (Buonomo et al., 2013; Carozza et al., 2015; Veress, Bicsak and Rohacs, 2016).

The other program was the practical measurements of the infrared radiation of engine – airframe sections of the aircraft demonstrators equipped by small gas turbine developed by ESPOSA project.

The aircraft infrared simulation is based on the coupled multiphisical (numerical fluid dynamics - CFD and heat transfer simulation) and / or multi-disciplinary models (including the chemical equations defining the burning processes and contents of the exhaust gases). Fig. 7 shows the applied simulation methodology.

The applied computational fluid dynamics simulations couple flow and thermal fields, solving the thermal conduction inside the nacelle wall (conjugate heat transfer analysis) due to the presence of the engine hot components and taking into account for nacelle cooling/ventilation system (Buonomo et al., 2013). The CFD analysis with proper boundary conditions at engine surface and nacelle wall considers the both convective and radiative heat transfer. Three-dimensional CFD calculations were performed by solving the Reynolds-averaged Navier-Stokes (RANS) equations. By use of Fluent code, the density-based flow solver and the standard SST (Shear-Stress Transport) k-ω model for turbulence were employed. In addition, the radiative exchange between engine and nacelle was also taken into account, by using the Discrete Ordinate model (Buonomo, 2013).
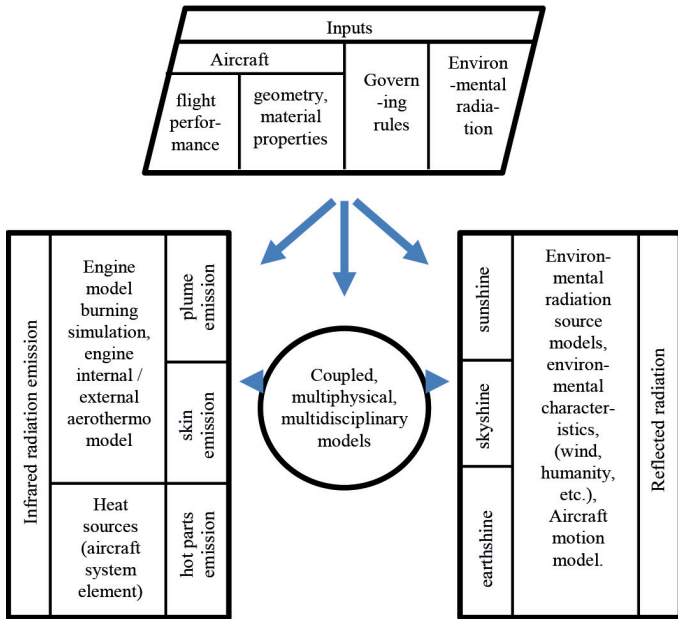
Fig. 7 Aircraft infrared radiation simulation methodology

6 Theoretical investigations

The ESPOSA (2016) project had resulted to implementing the developed small gas turbines on several small aircraft demonstrators. One of them is the EM-11 ORKA aircraft designed and manufactured by Margański and Mysłowski. This type was originally designed and built with two piston engine in pusher configuration, but was redesigned later and equipped with two TP-100 turbine engine designed and manufactured by PBS Velká Bíteš. The aircraft is a high wing, 4 seated aircraft, with retractable tricycle landing gear arrangement, and pusher propeller configuration (image of this aircraft is used in Fig. 1).

The another aircraft was a low wing, 4 seated I-31T aircraft (Fig. 8) designed by the Institute of Aviation in Warsaw and equipped with TP-100 turbine engine, too.

Fig. 8 The ESPOSA aircraft – demonstrator I-31T

According to the installation (2016) manual the maximum allowed operational temperatures for the TP-100 are given in Fig. 9. The Figure shows the hot sections that heat the nacelle elements.

The Figs. 10 and 11 demonstrate the results of the theoretical investigations.

The Fig. 10 shows the static temperature distribution on the nacelle surface of EM-11 ORKA aircraft (Buonomo et al., 2013) determined for cruise condition, namely for flight with cruise speed 87.445 m/s at 2750 m. At this level the air temperature equals to 268 K. The radiative heat transfer contribution had been taken into account, too. Its influence is in expected areas of the nacelle close to the hottest part of the engine. Further, no influence is foreseen in the nacelle parts far enough from engine and where forced convection effectiveness prevails, as the combustion air intake, at the lower front face of nacelle. The maximum temperature value (about 380 K) is reached close to the engine pipes and gas generator zone. This maximum temperature is close to maximum allowable one by component materials of nacelle skin (Buonomo et al., 2013).
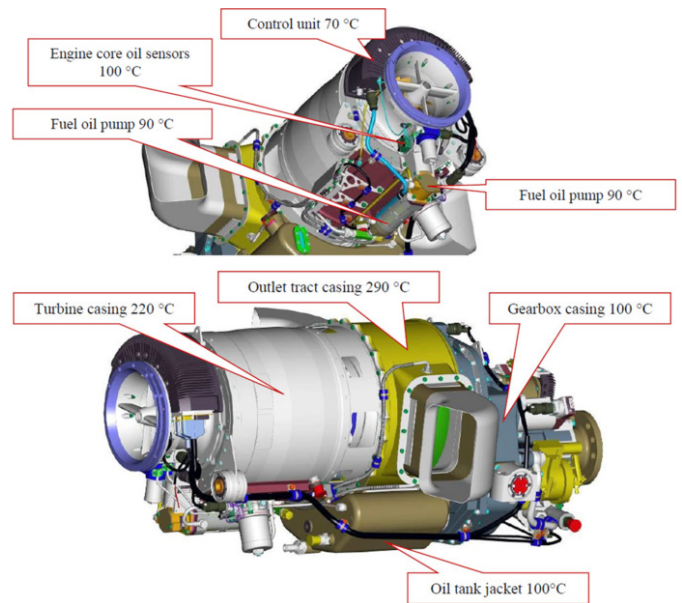

Fig. 9 Static temperature (K) contour of nacelle of EM-11 ORKA aircraft (Buonomo et al., 2013)
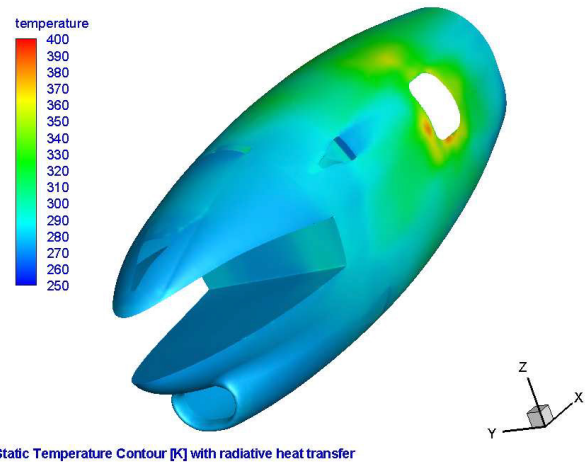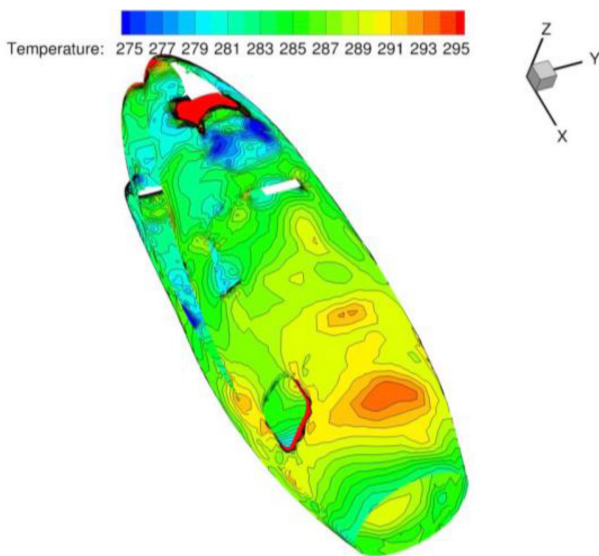

Fig. 10 Static temperature (K) contour of nacelle of EM-11 ORKA aircraft (Buonomo et al., 2013)

The Fig. 11 shows the wall temperature contours of nacelle of the same EM-11 ORKA aircraft for the engine idle condition (Carozza et al., 2015). For easier evaluation of the results the idle condition was chosen as 101325 Pa air pressure and 300 K air temperature. The propeller effects had been taken into account. (Carozza et al., 2015). Generally, the propeller may reduce the skin temperature up to 35 degree (Carozza et al., 2015). This fact explains the relatively low temperatures on nacelle surface.

As it can be recognized from Figs. 10 and 11 difference in maximum nacelle wall temperature for cruise and idle condition reaches 100 degree. However, the zones of the maximum temperatures are very small.
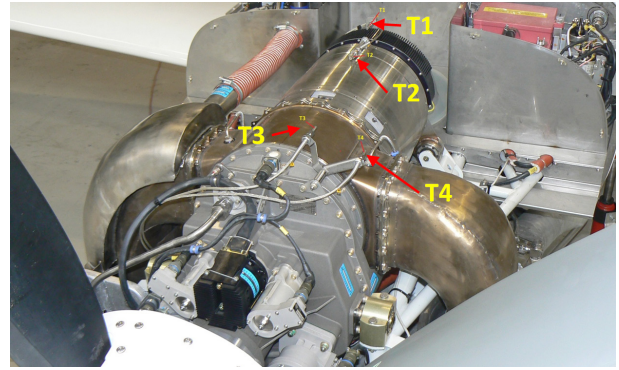

Fig. 12 Thermocouples under the nacelle

Fig. 11 Wall temperature (K) contours in case of engine idle condition and taking into the propeller effects (Carozza et al., 2015)

Fig. 13 Measurement condition
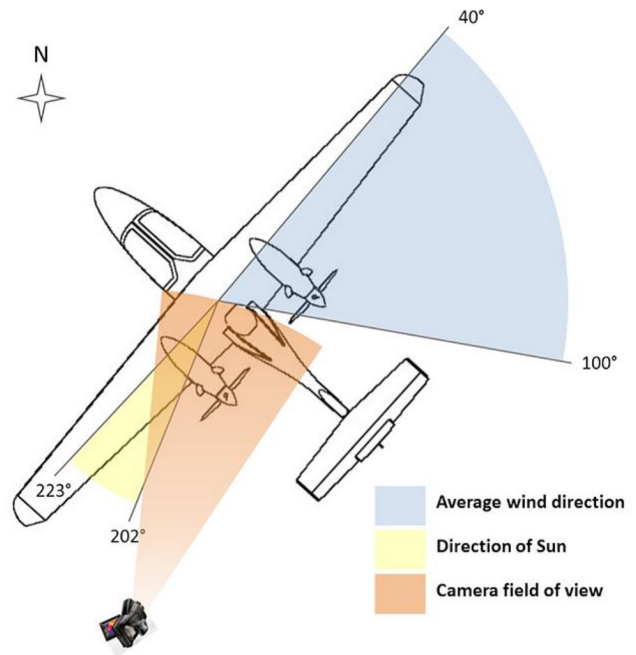
7 Measurements

ESPOSA aircraft demonstrators EM-11 OKRA and I-31 T (see Figs. 1 and 8) were applied in practical measurements of the infrared radiation of engine - airframe sections. The engine ground tests were measured. A Testo 885-2 thermal imager was used. This 320 x 240 pixel camera records the infrared radiation of spectral range 7.5 – 14 μm, by image refresh rate 33 Hz.

During measurements the engine parameters (frequency of rotation, exhaust gas temperature, oil temperature) and temperatures under nacelle by use of thermocouples (T1 - put close to the engine control unit, T2 - near the top of the engine cover, around the gas generator, near the inner surface of the mask, T3 – near the generator over the gearbox and T4 – near the fuel oil pump (see Fig. 12)) were registered, too, for supporting the further evaluation of the theoretical studies and practical measurements.

The quality of evaluation depends on the measuring situation as position of sun, wind direction, humidity, etc., too. The Fig. 13 shows the position of the investigated aircraft EM-11 OKRA during the test.

The Fig. 14 presents images recorded during the measurements. The left engine was started at 2:47 PM, i.e. at 46020 sec of the given day. The test was finished at 4:08 PM. the test included the series of changes in operational condition as it given in Table 2. So, the Fig. 14 shows images for engine start, taxiing, idling, take-off, max cruising, cruising, approach, take-off, stopping engine regimes.

Table 2 Engine test process

Time	Engine operational condition	Time	Engine operational condition
46020	Left engine start	49680	Approach
46200	Left engine warm up	49740	Take-off
46440	Right engine warm up	49860	Approach
46620	Taxiing	49920	Taxiing
46920	Idling	50220	Engines stop
47520	Take-off	50280	Cooling
47880	Max. Cruising power	50880	End of measurement
48660	Cruising power		
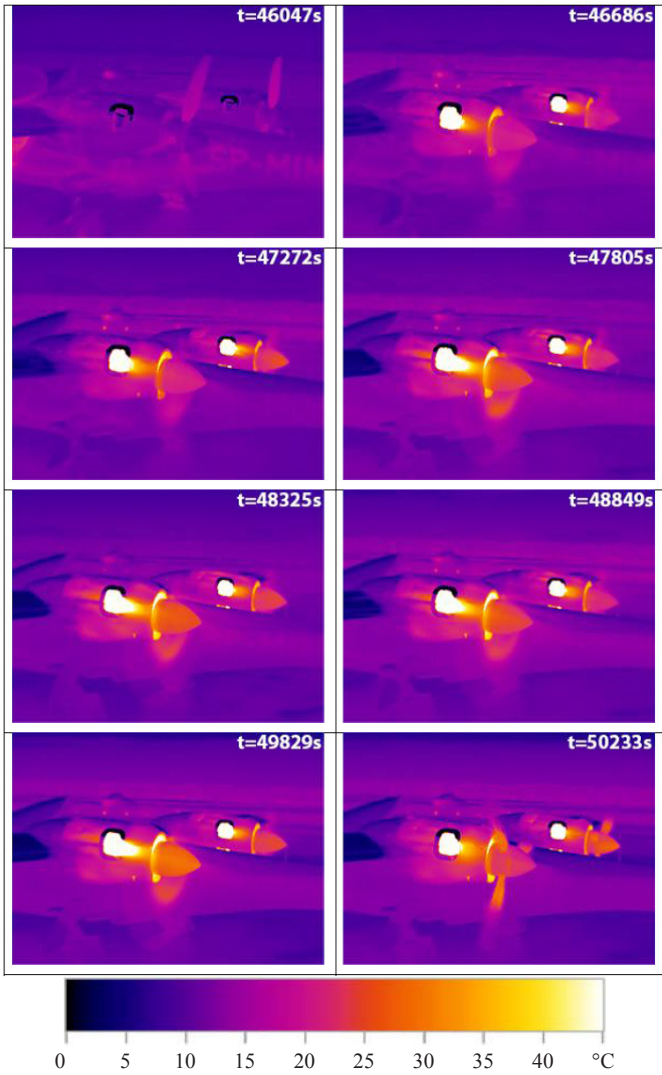
Fig. 14 Examples of infrared images recorded during an engine test

inaccurate. However there is a well detectable zone with heating effect of exhaust gas on nacelle and propellers.
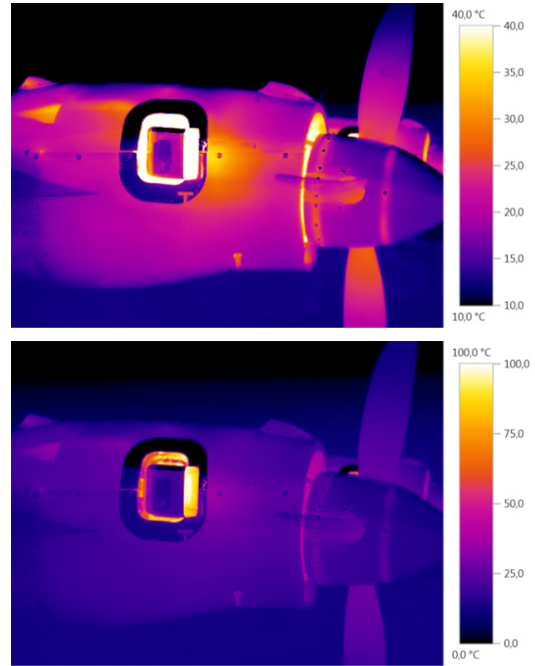

Fig. 15 Left side of left engine nacelle radiation with different temperature scales

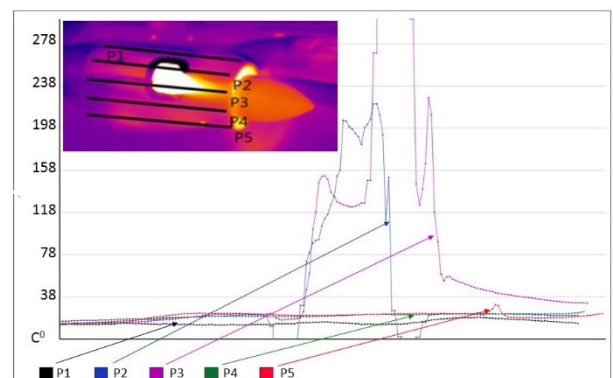**Fig. 16** The exhaust pipe on left engine of aircraft AM-11 OKRA

Fig. 17 Changes in wall temperature along the chosen reference lines

In Fig. 15, there is the same image showing the thermal condition of the left engine nacelle after engine test with use of two different temperature scales. As it can be seen, the hottest part of nacelle has appeared around the engine exhaust tube (see Fig. 16). The maximum temperature may over 100 ºC that is well correlating with the theoretical calculations (see Figure 10). The investigated engine is a turboprop engine; therefore the exhaust plume has not considerable thermal radiation. The left end of the exhaust pipe has top radiation, because the infrared camera looks into the pipe (as it can be understood from comparison the pictures of Fig. 15 and Fig. 16. On the same time, the exhaust plume heats the nacelle in zone after exhaust pipe (see upper image in Fig. 15).

The recorded images had been used for determining the temperature distribution on the nacelle surface. The changes in nacelle surface temperature along the chosen reference lines in case of middle cruise regime are presented in Fig. 17. Horizontal axis represents the length of line in pixels. Every point on the plot represents a pixel along the horizontal line, from left end to the right end. P2 and P3 lines are going through the exhaust tube where the temperatures are considered

The Fig. 18 demonstrates the real dependence of infrared radiation on engine installation. There are following zones of high temperature. Upper air intake louvres, which make visible hot

parts of the engine. The exhaust pipe, with temperatures beyond the scale. The exhaust gases from the pipe heat the nose wheel and ground around and after nose wheel to the temperatures which seem to be extreme to rubber parts for longer period, as well as for asphalt. Prolonged static operations of the engine set for maximum continuous power during tests contributed to small chuckholes in the apron surface. And the latter, the exhaust from oil cooler, located in the rear bottom of the cowling with temperatures within the scale. Because the applied temperature scale, the temperature of the exhaust tube cannot be detected by use of this image, in reality. However, the tube temperature is much greater (in analogy to Fig. 15), but additional temperature measurement points located on the exhaust pipe and other points on the cowling indicated, that the fumes are not so hot to damage the composite structure of the hood.
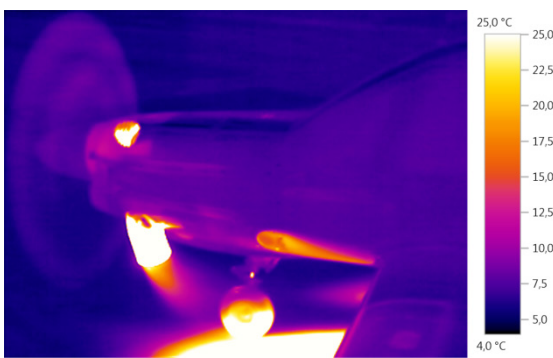

Fig. 18 Infrared images of nose section of ESPOSA aircraft demonstrator I-31 T

The Fig. 19 shows the thermal image of the aircraft I-31T noise section after 63 minutes ground test and 10 minutes cooling.

In Fig. 20 the temperature distribution shown at end of cruise phase along the chosen reference lines on nacelle wall of engine mounted in aircraft I-31T. This represents the best possible temperature distribution during flight. Although the temperatures are possibly greater than during flight, but the distribution is as close as possible. The flight test program of I-31T aeroplane included the measurements of temperature distribution on the engine cowling during all phases of flight in order to satisfy the requirements of CS.23.1041 and following points concerning engine cooling. The points were located on the inner and outer surfaces of the cowling in areas of the predicted high temeperature – exhaust traces, ECU, and gas generator. The analysis revealed that the most critical points on the engine cowling were located in the vicinity of exhaust gas traces. The temperatures on the inner surfaces of upper cowlings did not exceed 50 to 60 centigrade Celsius in general. However, recorded values reached temperatures up to 100 degrees Celsius in certain flight conditions. As well as may be noticed in the Figs. 18 and 19, after engine shut down the temperatures in measuring points increased radically.
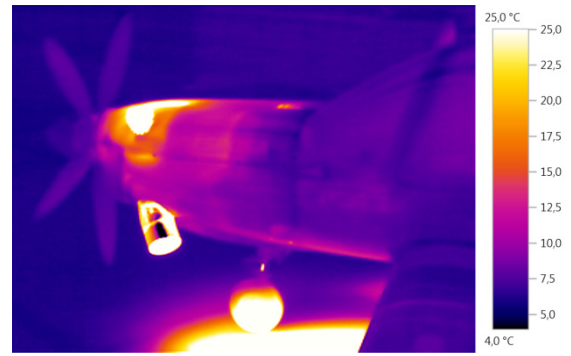

Fig. 19 Image after engine ground test and 10 minutes cooling (aircraft I-31 T)
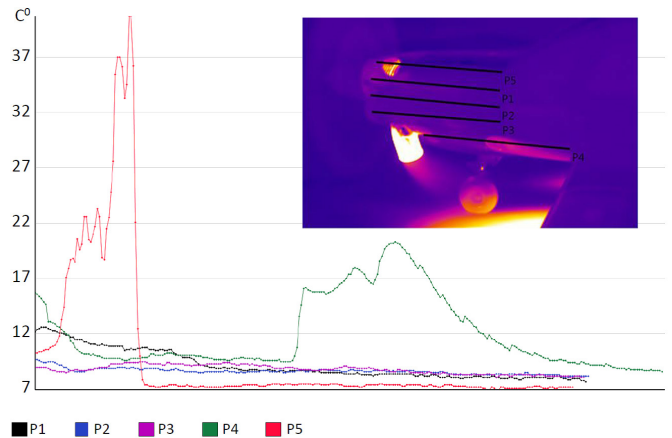

Fig. 20 Changes in nacelle wall temperature along the chosen reference lines for engine built into aircraft I-31 T

8 Conclusions

Probably, the ESPOSA (2016) project was the first large project developing and implementing a multi physical, namely aero and thermal optimization in integration of engine into the airframe. The goal was to minimize the aero-thermal losses for increasing the engines' effectivities and reducing the infrared radiations origin from engine - airframe structure. The study and optimization process were started by theoretical investigations resulting to development of a CFD methods for aero-thermal integration of engine into airframe. After it a special practical investigations were organized and realized.

The analysis of previous theoretical investigations and practical measurements of the aircraft infrared radiations as well as the theoretical results of the ESPOSA project allowed to define the condition and methodology for infrared radiation measurements of the aircraft demonstrators. The paper introduced the first systematic investigation of the small aircraft infrared radiation. The full engine ground test was measured. The measurements are fitted with theoretical investigations and show the possible improvements for reducing the infrared radiation origin from engine-airframe structure.

Acknowledgement

References

Andersson, M. (2002). *Derivation of equations used by the computer program SIGGE for calculating the IR-intensity.* FOI, Swedish Defence Research Agency, Methodology report, No. 1650-1942, Division of Aeronautics, FAA, Stockholm.

Bicsák, Gy., Hornyák A., Veress, A. (2012). Numerical Simulation of Combustion Processes in a Gas Turbine. In: Proceedings of the 9th International Conference on Mathematical Problems in Engineering, Aerospace and Sciences (ICNPAA), Vienna, Austria, Jun. 10 – 14, 2012. American Institute of Physics, 1493, pp. 140-148.

Boden, F., de Groot, K., Meyer, R., Bakunowicz, J., Rzucidło, P., Smusz, R., Szewczyk, M., Szumski, M. (2015). Flow and Structure Deformation Research of a Composite Glider in Flight Conditions. In: 46th Annual International Symposium of the Society of Flight Test Engineers 2015, Lancaster, California, USA, Sept.14 – 17, 2015. pp.138-147.

Bolckom, C., Feickert, A., Elias, B. (2004). Homeland security: protecting airliners from terrorist missiles. Congressional Research Service, Library of Congress, Washington DC. Order Code RL31741. [Online]. Available from: https://fas.org/irp/crs/RL31741.pdf [Accessed: 12th July 2016]

Buonomo, G., Musto, M., Bianco, N., Rotondo, G., Pezzella, G., Mingione, G. (2013). Aerothermal analysis of an aircraft nacelle in the framework of a fully coupled approach. In: XXII conference of the Italian Association of Aeronautics and Astronautics, Napoli, Sept. 9-13, 2013. [Online]. Available from: https://www.researchgate.net/publication/263733250_AEROTHERMAL_ANALYSIS_OF_AN_AIRCRAFT_NACELLE_IN_THE_FRAMEWORK_OF_A_FULLY_COUPLED_APPROACH [Accessed: 22nd May 2016]

Capps, W. L., Powlette, D., Tate, S. E., Amick, G. S., Stowall, D., Hustea, F. (1983). The aircraft infrared measurements guide, Joint Technical Coordinating group on Aircraft Survivability (JTCG/AS). Report Number JTCG/AS-81-C-002. [Online]. Available from: http://www.dtic.mil/dtic/tr/fulltext/u2/a132598.pdf [Accessed: 30th May 2016]

Carozza, A., Mignione, G., Serino, G., Pezella, G. (2015). Thermal investigation of a naccele internal and external fields in pusher configuration. In: XXIII Conference of the Italian Association of Aeronautics and Astronautics, Torino, Italy. [Online]. Available from: https://www.researchgate.net/publication/284184148 [Accessed: 22nd May 2016]

Coiro, E., Chatelard, C., Durand, G., Langlois, S., Martinenq, J. P. (2012). Experimental validation of an aircraft infrared signature code for commercial airliners. In: 43rd AIAA Thermophysics Conference, New Orleans, Lousiana, USA, June 25, 2012, pp. 1269-1283. https://doi.org/10.2514/6.2012-3190

Davis, W. R., Thompson, J. (2002). Developing an IR signature specification for military platforms using modern simulation techniques. In: Annual SMI Pursuit of Stealth Conference, London, 2002.

ESPOSA (2016). Efficient Systems and Propulsion for Small Aircraft. [Online]. Available from: http://www.esposa-project.eu/en/efficient-systems-and-propulsion-for-small-aircraft-2.html [Accessed: 12th June 2016]

Hendrick, P., Gobeil, M., Morabito, A., Roba, Ch., Carozza, A., Mingione, G., Pezzella, G. (2015). Installation issues of a small turboshaft engine into a light helicopter. In: AVT-230 Specialists Meeting on Advanced Aircraft Propulsion Systems. Rzeszów, Poland, April 20-22, 2015.

Henini, M., Razegni, M. (2002). *Handbook of infrared detection technologies.* Elsevier, Science Ltd.

Holmes, B. J., Durhan, M. H., Tarry, S. E. (2004). Small Aircraft Transportation System Concept and Technologies. *Journal of Aircraft.* 41(1), pp. 26–35. https://doi.org/10.2514/1.3257

Huang, W., Ji, H.-H. (2014). Investigation of a two-dimensional hot jet's infrared radiation using four different turbulence models. *Mathematical Problems in Engineering.* 2014, pp. 1-12. https://doi.org/10.1155/2014/298186

Huang, W., Ji, H.-H. (2016). Impact of Background radiation on the Long Wave Infrared radiation characteristics of Aircraft at High Altitude. *Defence Science Journal.* 66(1), pp. 51-56. https://doi.org/10.14429/dsj.66.8090

Hudson, Jr R. D. (1969). *Infrared system engineering.* 1st ed. New York, Wiley

Iannarilli, Jr F. J., Wohlers, M. R. (1991). End-to-end scenariogenerating model for IRST performance analysis. In: Proceedings of SPIE - The International Society for Optical Engineering: signal and data processing of small targets. Vol. 1481, pp. 187–197. Bellingham, WA, USA, SPIE.

Installation (2016). Manual for Turboprop Engine TP100. První brněnská strojírna Velká Bíteš, a.s

Jianwei, L., Qiang, W. (2009). Aircraft-skin infrared characterisitcs modeling and analysis. *Chinese Journal of Aeronautics.* 22, pp. 493 - 497. https://doi.org/10.1016/S1000-9361(08)60131-4

Jingzhou, Z., Chengxiong, P., Yong, S. (2014). Progress in helicopter infrared signature suppression. *Chinese Journal of Aeronautics.* 27(2), pp. 189-199. https://doi.org/10.1016/j.cja.2014.02.007

Joyner, T., Makar, B., Jacobs, S., McKee, D., Stanley, F. (1998). Joint Navy and Air Force Infrared Sensor Stimulator (IRSS) program for Installed Systems Test Facilities (ISTFs). Open Archive Initiative, Defense technical Information Center. [Online]. Available from: http://oai.dtic.mil/oai/oai?verb=getRecord&metadataPrefix=html&identifier=ADA375775 [Accessed: 6th June 2016]

Mahulikar, S. P., Sane, S. K., Gaitonde, U. N., Marathe, A. G. (2001). Numerical studies of infrared signature levels of complete aircraft. *The Aeronautical Journal.* 105(1046), pp. 185–192. https://doi.org/10.1017/S0001924000025422

Mahulikar, S. P., Kolhe, P. S., Rao, G. A. (2005). Skin temperature prediction of aircraft rear fuselage with multimode thermal model. *Journal of Thermophysics and Heat Transfer.* 19(1), pp. 114–124. https://doi.org/10.2514/1.6299

Mahulikar, S. P., Rao, G. A., Kolhe, P. S. (2006). Infrared signatures of low flying aircraft and their rear fuselage skin's emissivity optimisation. *Journal of Aircraft.* 43(1), pp. 226–232. https://doi.org/10.2514/1.15365

Mahulikar, S. P., Sonawe, H. R., Rao, A. (2007). Infrared signture studies of aero-saspace vehicles. *Progress in Aerospace Sciences.* 43(7-8), pp. 218-245. https://doi.org/10.1016/j.paerosci.2007.06.002

McGlynn, J. D., Auerbach, S. P. (1997). IR signature prediction errors for skin-heated aerial targets. In: Proceedings of SPIE - The International Society for Optical Engineering, Targets and backgrounds: characterization and representation - III. 3062, pp. 22-30. Bellingham, WA, USA: SPIE. https://doi.org/10.1117/12.276690

Miller, R. (1993). EO/IR modeling of a generic aircraft. *Proceedings of SPIE 1969, Infrared Imaging Systems: Design, Analysis, Modeling, and Testing IV.* 150, pp. 150-156. https://doi.org/10.1117/12.154711

Minkina, W., Dudzik, S. (2009). *Infrared Thermography: Errors and Uncertainties.* Willey.

Noah, M., Kristl, J., Schroeder, J., Sandford, B. P. (1991). NIRATAM-NATO infrared air target model. In: Proceedings of SPIE, Surveillance Technologies. Vol. 1479, pp. 275-282.

Oravecz J., Kováts L. D., Rohacs J. (2000). Harci helikopterek infravörös sugárzásának csökkentése. (Reducing the Infrared radiation of the military helicopters.) *Katonai Logisztika.* 8(2), pp. 221-237.

Palme, R., Siket, Zs., Gati, B., Rohacs, J. (2010). Non-cooperative target classification, with use of their measured motion kinematics. In: Proceedings of the 12th Mini Conference on Vehicle System Dynamics, Identification and Anomalies, Nov. 8-10, 2010. Budapest, Hungary, (Zobory, I. (ed.)), BME Budapest 2012, pp. 369-384.

Pan, C., Zhang, J., Shan, Y. (2011). Modeling and analysis of helicopter thermal and infrared radiation. *Chinese Journal of Aeronautics.* 24, pp. 558-567. https://doi.org/10.1016/S1000-9361(11)60065-4

Perotoni, M. B., Andrade, L. A. (2011). Numerical evaluation of an air-to-air missile radar cross section signature at X-band. *Journal of Aerospace Technology and Management.* 3(3), pp. 287-294. https://doi.org/10.5028/jatm.2011.03034111

Piwek, K., Wiśniowski, W. (2016). Small air transport aircraft entry requirements evoked by FlightPath 2050. *Aircraft Engineering and Aerospace Technology.* 88(2), pp. 341-347. https://doi.org/10.1108/AEAT-02-2015-0065

Pocket (2012) Guide Thermography Theory – Practical Application. Testo AG. [Online]. Available from: https://www.testo-international.com/media/local_media/870downloads/pocket_guide_thermography/pocket_guide_ti_04_2013_en.pdf [Accessed: 14th November 2014]

Rao, G. A., Mahulikar, S. P. (2005). Effect of atmospheric transmission and radiance on aircraft infrared signatures. *Journal of Aircraft.* 42(4), pp. 1046-1054. https://doi.org/10.2514/1.7515

Rogalski, A. (2012). History of infrared detectors. *Opto-Electronics Review.* 20(3), pp. 279-308. https://doi.org/10.2478/s11772-012-0037-7

Rohacs, D. (2007a). *Noon-Linear Prediction Model for the European Small Aircraft Accessibility for 2020.* PhD Thesis, Budapest University of Technology and Economics, Budapest, Hungary.

Rohacs, D. (2007b). Non-linear probabilistic prediction of the small aircraft accessibility: A European model for the piston, turboprop and jet aircraft. In: Transport Means, Confeerence Proceedings. pp. 43-46.

Rohacs, J., Palme, R., Siket, Zs. (2010). Non-Cooperative Target Classification to Improve Safety on Airport Approach and Departure Domain. In: Proceedings of the International Symposium on Safety Science and Technology (2010 ISSST). Hangzou, China, Oct. 26-29, 2010, pp. 1931-1944.

Rothman, L. S., Gordon, I. E., Babikov, Y., Barbe, A., ChrisBenner, D., Bernath, P. F., Birk, M., Bizzocchi, L., Boudon, V., Brown, L. R., Campargue, A., Chance, K., Cohen, E. A., Coudert, L. H., Devi, V. M., Drouin, B. J., Fayt, A., Flaud, J.-M., Gamache, R. R., Harrison, J. J., Hartmann, J.-M., Hill, C., Hodges, J. T., Jacquemart, D., Jolly, A., Lamouroux, J., LeRoy, R. J., Li, G., Long, D. A., Lyulin, O. M., Mackie, C. J., Massie, S. T., Mikhailenko, S., Müller, H. S. P., Naumenko, O. V., Nikitin, A. V., Orphal, J., Perevalov, V., Perrin, A., Polovtseva, E. R., Richard, C., Smith, M. A. H., Starikova, E., Sung, K., Tashkun, S., Tennyson, J., Toon, G. C., Tyuterev, VI. G., Wagner, G. (2013). The HITRAN 2012 Molecular Spectroscopic Database. *Journal of Quantitative Spectroscopy and Radiative Transfer.* 130, pp. 4-50. https://doi.org/10.1016/j.jqsrt.2013.07.002

Santos, R. A. T., Taranti, C. G. R., Alves, F. D. P., Olivera, J. E. B. (2007). Development of a methodology for infrared aircraft emission estimation. In: Progress in Electromagnetics Research Symposium 2007. Beijing, China, Mar. 26-30, 2007. pp. 663-668. [Online]. Available from: https://www.researchgate.net/publication/265281961_Development_of_a_Methodology_for_Infrared_Aircraft_Emission_Estimation [Accessed: 24th October 2014]

Siegel, R., Howell, J. R. (1972). *Thermal Radiation Heat Transfer.* McGraw-Hill.

Sweetman, B. (2003). The enemy down below. *Air Transport World.* 40, pp. 34-36.

Titterton, D. H. (2006). Development of infrared countermeasure technology and systems. In: Krier, A. (ed.) *Mid-infrared semiconductor optoelectronics.* (pp. 635-671). Springer-Verlag, Berlin,

Veress, A., Bicsak, Gy. Rohacs, D. (2016). Pressure loss and flow uniformity analysis of baseline and redesigned engine inlet duct for a small turboprop aircraft. In: Czech Aerospace Proceedings. No. 1., pp. 3-9. [Online]. Available from: http://vx439500.server37.viwefix.cz/magazines/inbrowser.aspx?id=48 [Accessed: 26th May 2016]

Waldman, G, Wootton, J. (1993). *Electro-optical systems performance modelling.* 1st ed. Artech House, Boston.

White, J. R. (2012). *Aircraft infrared principles, signitures, threats and countermeasures.* Naval Air Warfare Center Weapons Division, Point Mugu, Ca, US, NAWCWD TP 8773. [Online]. Available from: http://www.dtic.mil/cgi-bin/GetTRDoc?AD=ADA566304 [Accessed: 27th March 2015]

Willers, M. S., Willers, C. J. (2012). Key considerations in infrared simulations of the missile-aircraft engagement. In: *P*roceedings SPIE Volume 8543, Technologies for Optical Countermeasures IX (Ed. by Titterton, D. H., Richardson, M. A.) Edinburgh, United Kingdom. https://doi.org/10.1117/12.974801